PROCEEDINGS A

royalsocietypublishing.org/journal/rspa

Research

Cite this article: Pal D, Chakraborty S. 2019 New regimes of dispersion in microfluidics as mediated by travelling temperature waves. *Proc. R. Soc. A* **475**: 20190382.
http://dx.doi.org/10.1098/rspa.2019.0382

Received: 18 June 2019
Accepted: 3 September 2019

Subject Areas:
chemical engineering, fluid mechanics

Keywords:
dispersion, microfluidics, thermoviscous pumping, travelling temperature wave

Author for correspondence:
Suman Chakraborty
e-mail: suman@mech.iitkgp.ernet.in

Electronic supplementary material is available online at https://dx.doi.org/10.6084/m9.figshare.c.4688780.

THE ROYAL SOCIETY PUBLISHING

New regimes of dispersion in microfluidics as mediated by travelling temperature waves

Debashis Pal[1] and Suman Chakraborty[2]

[1]Aerospace Engineering and Applied Mechanics Department, Indian Institute of Engineering Science and Technology Shibpur, Howrah 711103, India
[2]Department of Mechanical Engineering, Indian Institute of Technology Kharagpur, Kharagpur 721302, India

DP, 0000-0001-7141-4516; SC, 0000-0002-5454-9766

We unveil new regimes of dispersion in miniaturized fluidic devices, by considering fluid flow triggered by a travelling temperature wave. When a temperature wave travels along a channel wall, it alters the density and viscosity of the adjacent fluid periodically. Successive expansion–contraction of the fluid volume through a spatio-temporally evolving viscosity field generates a net fluidic current. Based on the temporal evolution of the axial dispersion coefficient, new regimes of dispersion—such as a short-time 'oscillating regime' and a large-time 'stable regime'—have been identified, which are absent in traditionally addressed flows through miniaturized fluidic devices. Our analysis reveals that the oscillation of axial dispersion persists until the variance of species concentration becomes equal to half of the square of the wavelength of the thermal wave. The time period of oscillation in the dispersion coefficient turns out to be a unique function of the thermal wavelength and net flow velocity induced by thermoviscous pumping. The results of this study are likely to contribute towards the improvement of microscale systems that are subjected to periodic temperature variations, including microreactors and DNA amplification devices.

1. Introduction

Hydrodynamic dispersion implies natural spreading of species molecules/particles along the flow direction, the rationale for the spreading being related to the transverse variation of velocity for internal flows [1–9]. The shape of

the velocity profile in a channel depends largely on the driving agent—could be pressure gradient, electrokinetic force, motion of wall (shearing action) or some other means.

Thermoviscous expansion of a fluid along a travelling temperature wave employs a spatio-temporally varying temperature field as the flow actuating mechanism [10–12]. When a temperature wave travels along a channel wall, it alters the density and viscosity of the adjacent fluid periodically. Successive expansion–contraction of the fluid volume through a spatio-temporally evolving viscosity field generates a net fluidic current (known as mean flow) along the wall, opposite to the motion of the temperature wave. When the channel height (h) and the thermal penetration depth (δ_t) are of the same order, the mean or time-averaged flow yields a steady parabolic profile [12]; the instantaneous flow field, however, remains oscillatory.

Studies on hydrodynamic dispersion in the presence of an oscillating flow field include the classical works by Aris [13], Harris & Goren [14], Chatwin [15], Smith [16], Watson [17] and Yasuda [18], while somewhat more contemporary developments are reported in Hazra *et al.* [19], Bandyopadhyay & Mazumder [20], Ng [21] and Jansons [22]. Species dispersion under the influence of flow oscillation has drawn significant attention from researchers because of its wide range of applications, namely the spreading of tracers injected into pulsatile blood flow in cardiovascular systems [23–25], estuary tidal flow [26,27], studies on the artificial ventilation of the human lung [28–32] and transport of environmental contaminants [15,16,33,34]. In the context of microfluidics, the dispersion phenomenon has been studied extensively owing to its application in the area of micro-mixing, drug delivery, processing of biological samples, separation science and detection of chemical components [8,9,25,35–37]. Most of the reported studies on dispersion address isothermal flow actuated by conventional methods such as pressure gradient (pulsating or steady), oscillating wall and electrokinetic force, with the major focus on the prediction of the dispersion coefficient of the concerned species. Tripathi *et al.* [38] have shown that a time-periodic temperature field can enhance the dispersion of genomic DNA in a microfluidic polymerase chain reaction device to the extent of the dispersion caused by the pressure-driven flow. The processing of small bioparticles in narrow conduits using ultrasound acoustophoresis has numerous applications in medical science and in environmental and food analysis [39–42]. Consequently, there is a need to develop tools for engineering acoustic streaming patterns that allow for acoustic handling of small particles. Recent studies have shown that temperature-induced thermoviscous effects can control the acoustic radiation force and boundary-driven acoustic streaming in straight microchannels [43–45], leading to a significant increase in the magnitude of the streaming velocity. The presence of a species/bioparticles inside such channels is likely to cause dispersion.

Motivated by the above applications, we investigate here the dispersion of sample plugs in microchannels that are subjected to a travelling temperature wave. In this regard, it is necessary to recall that the celebrated Taylor dispersion essentially refers to an increase in the effective dispersion that arises from pressure-driven transport through a conduit in the so-called long-time limit [1,2,7]. This long-time analysis is only valid for times much larger than the characteristic diffusion time for the species (time scale for equilibration in the direction perpendicular to the flow, t_d). In the realm of microfluidics, the study of dispersion for relatively short times is even more important [8,46], as often the transport processes occur rapidly in microfluidic devices (alternatively, the conduits are short). In this article, we categorically focus on the short-time regime of dispersion, while the long-time limit is also investigated subsequently. We also recognize that, for simple cases of isothermal, pressure-driven or electrokinetic transport, analytical results for dispersion are available [8,9,47–52], while more complicated cases with temperature-dependent fluid property variations require full-scale numerical analysis.

In this paper, we provide a quantitative description of hydrodynamic dispersion by estimating the axial dispersivity or effective diffusivity (D_{eff}) of a species in a two-dimensional microfluidic channel in the presence of thermoviscous actuation. Unlike the pressure-driven oscillatory flow in a channel, the instantaneous flow field induced by thermoviscous expansion is not unidirectional. A fluctuating cross-stream velocity (v) exists. A non-zero transverse velocity (v) in conjunction with spatio-temporally varying flow property is likely to influence the transverse

(cross-stream) diffusion of a species, particularly in small observation time. To investigate the effects of such inherent unsteadiness on the dispersion of a sample, the concentration field is obtained by numerically solving the unsteady advection–diffusion equation for the species along with the conservation equations for mass, momentum and energy. The temporal evolution of axial dispersion coefficient (D_{eff}) has been estimated for a wide range of Péclet numbers (Pe). Based on the differences in the spreading behaviour of the sample, a short-time oscillating regime (when D_{eff} varies periodically with time) and a large-time stable regime (when D_{eff} becomes constant) are identified. The oscillating and the stable regimes are demarcated by a characteristic time based on the wavelength (λ) of the temperature wave and the variance of the concentration distribution. The time period of oscillation of D_{eff} has been determined accurately. The large-time D_{eff} data obtained from our analysis are found to be in good agreement with the long-time solution of Taylor dispersion for a flat plate channel.

2. Problem formulation and analysis

The problem geometry consists of a parallel plate microchannel having length L and thickness h, as shown in figure 1. Fluidic transport inside the channel is actuated by periodic thermoviscous expansion of the fluid, which is realized by virtue of identical temperature waves of amplitude ΔT and wavelength λ, travelling along both the top and bottom plates in the same direction at a constant speed c. The flow governing equations, i.e. the continuity, the Navier–Stokes equation and the energy conservation, are expressed as

$$\frac{\partial \rho}{\partial t} + \frac{\partial}{\partial x}(\rho u) + \frac{\partial}{\partial y}(\rho v) = 0, \tag{2.1}$$

$$\rho\left[\frac{\partial u}{\partial t} + u\frac{\partial u}{\partial x} + v\frac{\partial u}{\partial y}\right] = -\frac{\partial p}{\partial x} + \frac{\partial}{\partial x}\left[2\mu\left(\frac{\partial u}{\partial x} - \frac{1}{3}\nabla\cdot\boldsymbol{V}\right)\right] + \frac{\partial}{\partial y}\left[\mu\left(\frac{\partial u}{\partial y} + \frac{\partial v}{\partial x}\right)\right], \tag{2.2a}$$

$$\rho\left[\frac{\partial v}{\partial t} + u\frac{\partial v}{\partial x} + v\frac{\partial v}{\partial y}\right] = -\frac{\partial p}{\partial y} + \frac{\partial}{\partial x}\left[\mu\left(\frac{\partial v}{\partial x} + \frac{\partial u}{\partial y}\right)\right] + \frac{\partial}{\partial y}\left[2\mu\left(\frac{\partial v}{\partial y} - \frac{1}{3}\nabla\cdot\boldsymbol{V}\right)\right] \tag{2.2b}$$

and

$$\rho C_p\left[\frac{\partial T}{\partial t} + u\frac{\partial T}{\partial x} + v\frac{\partial T}{\partial y}\right] = \beta_T T\frac{\mathrm{D}p}{\mathrm{D}t} + \nabla\cdot(k\nabla T) + \Phi, \tag{2.3}$$

where p is pressure, T is temperature and u and v are the x-component and y-component of flow velocity, respectively. Symbols ρ, μ, k, C_p and β_T represent density, viscosity, thermal conductivity, constant pressure specific heat and thermal expansion coefficient of the fluid, respectively. Here, Φ is the viscous dissipation function. No-slip, no-penetration boundary conditions are assumed at the wall. No external pressure gradient is applied along the length of the channel. The travelling temperature wave thermal boundary conditions at both of the walls are incorporated through the following equation:

$$T_{\text{wall}} = T_0 + \Delta T\cos\left\{\frac{2\pi}{\lambda}(x + ct)\right\}. \tag{2.4}$$

The temperature oscillation causes successive expansion and contraction of the fluid, leading to localized pressure pulsation along with fluctuations in both axial and transverse velocities. An intricate interplay of temperature-dependent viscosity and density generates a net unidirectional flow (in a time-averaged sense) in a direction opposite to the direction of wave motion. The genesis of thermoviscous actuation and the length scales and the velocity scales associated with such phenomena are discussed elsewhere [12,53]; they are not repeated here for the sake of brevity. In order to study the dispersion phenomenon, a solute slug is introduced into the 'steady' mean flow induced by thermoviscous actuation.

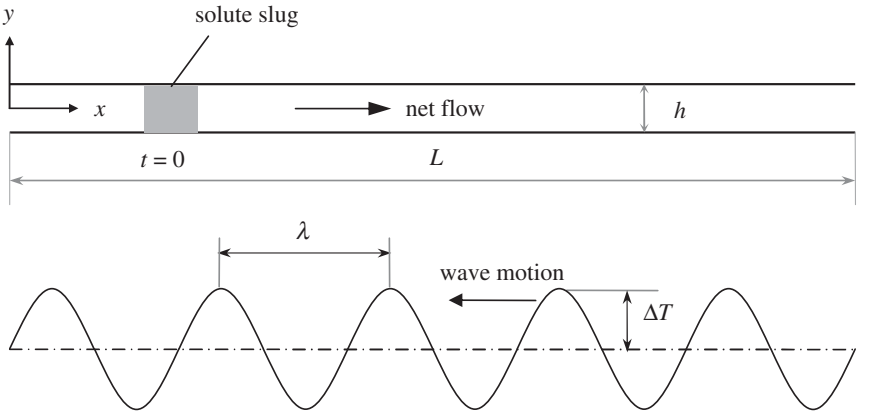

Figure 1. The parallel plate channel with a solute slug injected at time $t = 0$ into the 'steady' stream induced by thermoviscous actuation. The travelling temperature wave imposed on the wall boundary is also shown.

Accordingly, a conservation equation for species concentration is considered in a two-dimensional framework as

$$\frac{\partial C_s}{\partial t} + u\frac{\partial C_s}{\partial x} + v\frac{\partial C_s}{\partial y} = \frac{\partial}{\partial x}\left(D\frac{\partial C_s}{\partial x}\right) + \frac{\partial}{\partial y}\left(D\frac{\partial C_s}{\partial y}\right), \tag{2.5}$$

where C_s is the species concentration normalized with respect to the maximum concentration (C_∞) in the domain (so that $0 \le C_s \le 1$); and D is the temperature-dependent diffusivity of the species in the solvent fluid. Any appropriate temperature function $D(T)$ may be used to incorporate the diffusivity variation of the species. A familiar relationship for the molecular diffusion coefficient D is prescribed by the Stokes–Einstein equation [54,55], as

$$D(T) = \frac{k_B T}{6\pi\mu R_p}[\mathrm{m^2 s^{-1}}], \tag{2.6}$$

where μ is the temperature-dependent viscosity of the fluid; k_B and T are the Boltzmann constant and absolute temperature, respectively; and R_p is the effective hydrated radius of the solute particle (macromolecule). The above equation is valid when species molecules (solute particles) are small and of spherical shape.

(a) Assumptions and boundary conditions for species transport

In order to achieve a realistic picture of the species transport and dispersion, it is important to incorporate the effect of unsteadiness induced by wall temperature fluctuation, and, therefore, all the relevant properties are treated as functions of temperature. The major assumptions involved in the present analysis are as follows.

(i) The length-to-height ratio (L/h) of the capillary is large, so that a long-time assessment of dispersion (Taylor-type analysis) is possible.
(ii) The solute slug is injected in a fully developed stream, i.e. the net (time averaged) flow has already become periodically 'steady' at $t = 0$.
(iii) The solute particle size (R_p) is much smaller than the capillary size (h).
(iv) The solute is non-reacting.
(v) No wall interaction of the solute is allowed (no mass exchange, etc.).

The transport equation for species concentration (equation (2.5)) is therefore subject to the following boundary conditions ($t \ge 0$).

(i) Symmetry on the centreline, i.e. $\partial C_s/\partial y = 0$ at $y = 0$.
(ii) No flux of species at the wall, i.e. $\partial C_s/\partial y = 0$ at $y = \pm h/2$.
(iii) Zero concentration at the inlet and exit (far away), i.e. $C_s = 0$ at $x = \pm L/2$.

In the region where the solute is injected (figure 1), normalized species concentration $C_s = 1$ initially ($t = 0$). In the rest of the domain, $C_s = 0$ at $t = 0$.

(b) Axial dispersion coefficient, D_{eff}

The dispersion or spreading of a species in a channel is a combined consequence of stretching of the species band (due to convection-induced shear) and molecular diffusion in both the axial and transverse directions. In the analysis of hydrodynamic dispersion, traditionally, the mass diffusion Peclet number (Pe) emerges as a key governing parameter. Based on the cross-sectional average of net velocity $\overline{U}$ and channel height h, a mean Péclet number (Pe_0) is customarily defined as

$$\text{Pe}_0 = \frac{\overline{U}h}{D_0},$$

where D_0 is the mean molecular diffusivity of the species evaluated at the mean temperature T_0 (from equation (2.6)), and is given by

$$D_0 = \frac{k_B T_0}{6\pi\mu_0 R_p},$$

where μ_0 is the viscosity at T_0.

The Peclet number signifies the relative importance of convection to the molecular diffusion of species. The transport of a species with diffusion coefficient D_0 in the background fluid through a channel of thickness h yields a characteristic time for cross-channel diffusion $t_d = h^2/D_0$. If l_C is the characteristic length over which there is an appreciable concentration change in the axial direction, then the length-scale ratio h/l_C characterizes the relative strength of transverse diffusion to axial diffusion. In pressure-driven transport, there is a significant difference in the spreading behaviour of the solute shortly after its injection and after several diffusion times (t_d) have elapsed after its injection. Accordingly, based on the rate at which the solute spreads, two separate regimes are defined—a short-time regime or ballistic regime ($t \ll t_d$), and a long-time regime ($t \gg t_d$). The latter has been a traditional focus area outside the realm of microfluidics. However, species transport in microfluidics can often be fast enough for the short-time regime to be appropriate. Evidently, in the short-time regime, the cross-channel species diffusion is incomplete and is yet to take the full-fledged effect.

In classical Poiseuille flow, at large time, l_C is considerably greater than the transverse dimension, h [1,2]. When the Peclet number is very high ($\text{Pe} \gg l_C/h$), it turns out that the species transport is governed primarily by advection, and this regime is appropriately called the pure advection regime. A moderately high Peclet number ($1 \ll \text{Pe} \ll l_C/h$) gives way to the so-called Taylor–Aris regime, in which the species band (mixed zone) apparently grows in length, and equation (2.5) may be approximated as a simple one-dimensional equation involving the cross-sectional average of species concentration, $\overline{C_s}(x,t)$, as

$$\frac{\partial \overline{C_s}}{\partial t} + \overline{U}\frac{\partial \overline{C_s}}{\partial x} = D_{\text{eff}}\frac{\partial^2 \overline{C_s}}{\partial x^2}. \tag{2.7}$$

Here, D_{eff} is a 'phenomenological coefficient' characterizing the axial broadening of the mixed zone, and is subsequently called the Taylor–Aris dispersion coefficient. Equation (2.7) shows that the dispersion of a solute in a conduit may now be characterized by an unsteady diffusion process with an effective diffusivity or axial dispersivity equalling D_{eff}. The axial dispersivity is found to

be a function of Peclet number (Pe) and molecular diffusivity (D) and is usually given by

$$D_{\text{eff}} = D(1 + \alpha \text{Pe}^2), \tag{2.8}$$

where α is a parameter that depends on the geometry and flow boundary conditions. Long-time solute dispersion in a parallel plate channel yields $\alpha = 1/210$ [47]. It is imperative to mention here that the Poiseuille flow is isothermal and strictly unidirectional ($v = 0$).

Aris [3] put Taylor's theory [1,2] into a more general and rigorous theoretical framework, by pointing out that the main quantity of interest (i.e. D_{eff}) may be computed from the axial variance of species concentration distribution, which is nothing but the second statistical moment of the distribution about the axial coordinate around its centroid. The 'zeroth moment' is the fraction of analyte at the instant, and the 'first moment' is the axial position of the centroid of the analyte distribution. Accordingly, the variance of concentration distribution is estimated by

$$\sigma^2(t) = \langle x^2 \rangle(t) - \langle x \rangle^2(t), \tag{2.9}$$

where the quantity $\langle x^n \rangle(t)$ is a measure of the nth moment of the distribution and is quantified in a two-dimensional framework as

$$\langle x^n \rangle(t) = \frac{\int_{-\infty}^{+\infty} x^n \left\{ \int_{-h/2}^{+h/2} C_s(x, y, t) \mathrm{d}y \right\} \mathrm{d}x}{\int_{-\infty}^{+\infty} \left\{ \int_{-h/2}^{+h/2} C_s(x, y, t) \mathrm{d}y \right\} \mathrm{d}x}. \tag{2.10}$$

While the innermost integration in the above equation represents the cross-sectional average of concentration, $\langle x \rangle(t)$ essentially implies the x-coordinate location of the centroid of the distribution. Thus, to obtain the variance, the zeroth and first-order local moments have to be known first. Following Aris's method of moments [3,9], the time-dependent effective dispersion coefficient, $D_{\text{eff}}(t)$, is defined as

$$D_{\text{eff}}(t) = \frac{1}{2} \frac{\mathrm{d}}{\mathrm{d}t} [\sigma^2(t)], \tag{2.11}$$

which tends to a constant value in the long-time limit.

In this paper, thermoviscous expansion of the fluid induces high-frequency property (ρ, μ, u, v, p, etc.) fluctuations with typical time period (λ/c) in the range 10^{-3}s to 10^{-5}s, as dictated by the frequency of the temperature wave. While an intricate interplay between such property fluctuations yields a 'steady' unidirectional mean (time-averaged) flow, the effective dispersion coefficient is likely to get altered by the spatio-temporal property variations. In a microchannel, the extent of the fluid layer affected by periodic thermal fluctuations at the wall is characterized by a length scale called the thermal penetration depth, δ_t ($= \sqrt{\alpha_0 \lambda / c}$, where α_0 is the thermal diffusivity at mean temperature T_0) [12]. When the channel height and the thermal penetration length scale are of the same order ($h \sim \delta_t$), thermal perturbation is felt throughout the cross-section of the channel and the mean flow resembles the classical Poiseuille profile. However, unlike traditional pressure-driven flow (both constant and oscillating pressure gradient), the instantaneous flow field here is not unidirectional. A fluctuating transverse velocity v exists. It is, therefore, important to examine how and to what extent the inherent unsteadiness of the flow field—imposed by the thermal wave—affects the dispersion characteristics of the solute, particularly in small observation time. Such a time scale is important in microfluidics as channel lengths are typically small. To investigate the effect of thermoviscous expansion on dispersion, thus, full-scale numerical solutions of the relevant transport equations are necessary.

3. Numerical simulation

In an effort to provide a proper quantitative description of the time-evolving concentration field, comprehensive computational fluid dynamic (CFD) simulations of the physical problem under consideration have been carried out by employing a control volume-based finite difference method [56]. The computational domain consists of a rectangular region ($L \times h$), the top and bottom sides of which represent the walls of the channel (figure 1). The length of the domain is

Table 1. Diffusivities of various species in water [60].

particle (tracer)	characteristic diffusivity ($m^2\ s^{-1}$)
solute ion	2×10^{-9}
small protein	4×10^{-11}
virus	2×10^{-12}

much larger than the channel height and the wavelength of the thermal wave (i.e. $L \gg h, \lambda$). At the outset, only flow governing equations (equations (2.1–2.3)) are solved numerically until the net flow becomes 'steady' and fully developed (net velocity does not vary with t and x any longer). The solute slug is injected in the channel at this moment (set this instant as $t = 0$) and an unsteady-state solution of the species transport equation (equation (2.5)) is started in conjunction with the mass, momentum and energy equations (equations (2.1–2.3)). Both the top and bottom walls are subjected to the travelling temperature wave thermal boundary condition as per equation (2.4). The discretized system of linear algebraic equations is solved by employing a point-implicit (Gauss–Seidel) solver. A coupling between pressure and velocity is accomplished by using the Pressure Implicit with Splitting of Operators (PISO) algorithm [57]. To get rid of 'false diffusion', the advection term in the species transport equation (equation (2.5)) is discretized using the higher order Quadratic Upstream Interpolation for Convective Kinematics (QUICK) scheme [57]. Time integration is performed by incorporating a fully implicit scheme which is also unconditionally stable irrespective of time-step size. Nevertheless, the time-step size is chosen on the basis of the periodic time scale (λ/c) of the thermal wave as that is the smallest time scale involved.

The species diffusivity D is modelled by employing equation (2.6). In order to achieve a realistic picture of species transport and dispersion, temperature-dependent density (ρ), viscosity (μ) and thermal conductivity (k) are evaluated using appropriate empirical relations (assuming the solvent to be water) [58,59]

$$\rho = 1000 - 0.0178|T^{\circ}C - 4^{\circ}C|^{1.7}[\mathrm{kg\,m^{-3}}], \tag{3.1a}$$

$$\mu = 2.761 \times 10^{-6} \exp\left(\frac{1713}{T + 273}\right)[\mathrm{Pa\,s}] \tag{3.1b}$$

and

$$k = 0.61 + 0.0012(T - 25^{\circ}C)[\mathrm{W\,m^{-1}\,K^{-1}}]. \tag{3.1c}$$

It must be noted that temperature T in equations (3.1*a–c*) are expressed in °C. Equation (3.1*a*) is valid in the range $0^{\circ}C \leq T \leq 100^{\circ}C$, with $\pm 0.2\,\%$ error. With the appropriate choice of wavelength λ and wave speed c, the stipulated height to thermal penetration depth ratio (say, h/δ_t close to 1) is maintained. The mean Peclet number (Pe_0) is altered by varying the channel height h, wave speed c, amplitude ΔT (c and ΔT are two parameters on which the net velocity scale is dependent [12]) and mean species diffusivity D_0. Typical diffusion coefficients of various species in water at room temperature (table 1) are considered as the input values of mean diffusivity. The time evolution of D_{eff} has been estimated from the numerically obtained concentration field using equations (2.9–2.11) for a wide range of Pe_0.

4. Results and discussions

In order to capture both short time-scale and large time-scale features of dispersion, numerical simulations are carried out for adequate flow time. The variance of concentration distribution (σ^2) and the effective axial dispersion coefficient (D_{eff}) have been computed from equations (2.9–2.11) by employing a Matlab program, in which the numerically obtained concentration, $C_s(x, y, t)$, is used as input data. The temporal evolution of D_{eff}, normalized by the mean diffusivity D_0, has been plotted for three distinct values of Pe_0 in figure 2. The channel height to thermal penetration depth ratio is kept close to 1 ($h/\delta_t = 0.82$). There is considerable difference in the dispersion

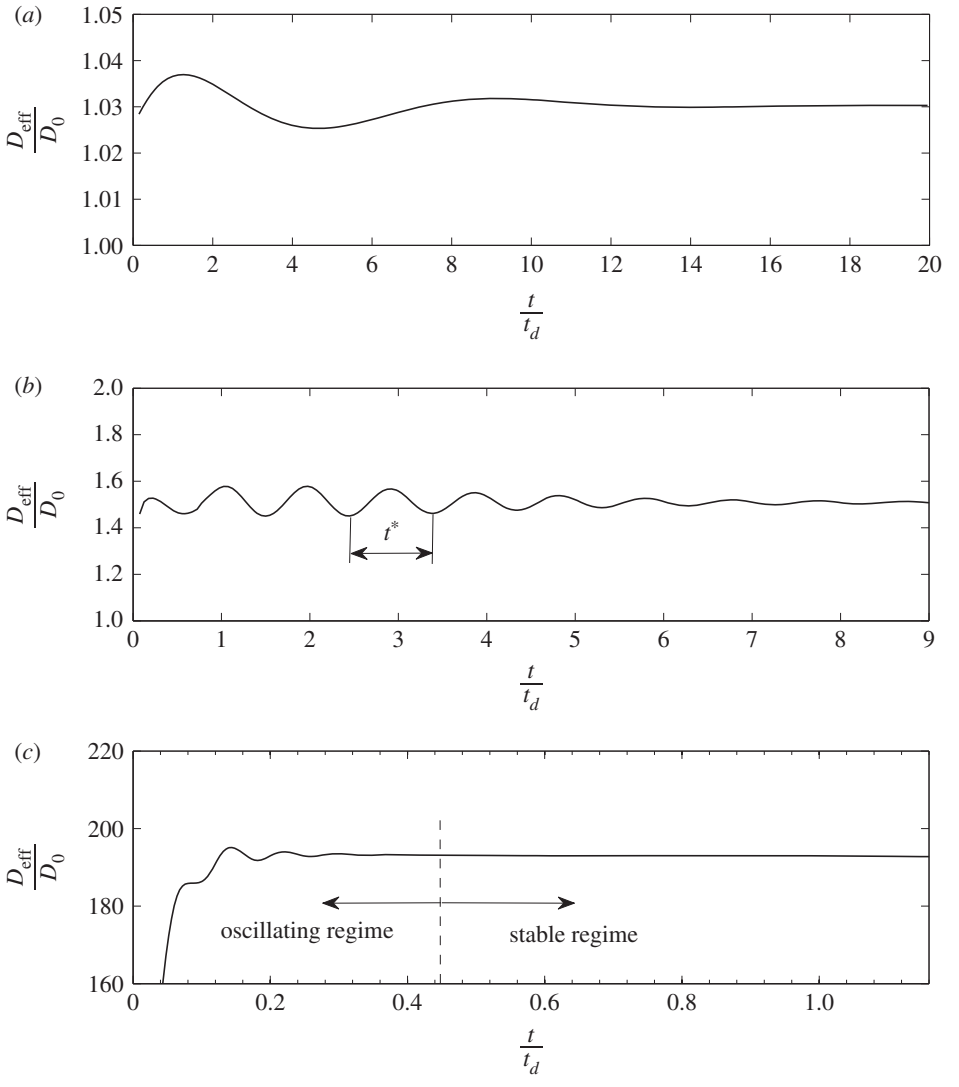

Figure 2. Time evolution of the axial dispersion coefficient (D_{eff}) for flow induced by thermoviscous actuation in a microchannel with $h = 10\ \mu\text{m}$ and $h/\delta_t = 0.82$. Case (*a*): $\text{Pe}_0 = 1.1$, $\lambda = 100\ \mu\text{m}$, $c = 0.1\ \text{m s}^{-1}$; case (*b*): $\text{Pe}_0 = 10.5$, $\lambda = 100\ \mu\text{m}$, $c = 0.1\ \text{m s}^{-1}$; and case (*c*): $\text{Pe}_0 = 210$, $\lambda = 200\ \mu\text{m}$, $c = 0.2\ \text{m s}^{-1}$ (the oscillating and stable regimes are identified from figure 3).

characteristics of the species shortly after its injection and after a long time has elapsed after its injection. Nevertheless, some universal trends are observed, regardless of the Pe_0 variation.

First, the D_{eff} oscillates periodically over a short time scale; however, as time elapses, it gradually subsides and becomes constant. For moderately high Peclet numbers (say, $1 < \text{Pe}_0 < 100$), the oscillation in the value of D_{eff} is observed until t equals several diffusion time scales ($t \approx 10\, t_d$ or more), as shown in figure 2*b*. When the Pe_0 is very high (say, $\text{Pe}_0 \geq 100$), the dispersivity oscillation dies away within a fraction of the diffusion time scale t_d, which is evident from figure 2*c*. Such a quick settlement of oscillation of D_{eff} may be attributed to the overall dominance of advection over diffusive transport at large Peclet number. Nevertheless, there are two distinct regimes irrespective of the Pe_0 value—a short-time oscillating regime and a large-time stable regime. The demarcation between these two regimes is not dictated by the diffusion time scale, t_d, though.

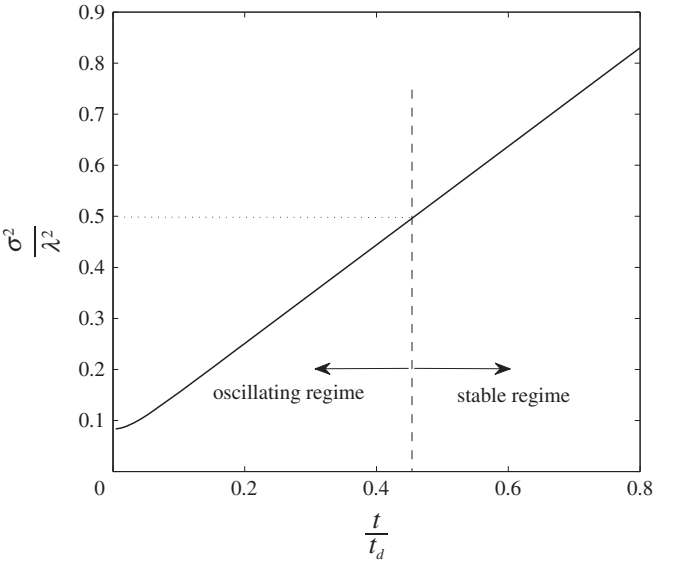

Figure 3. Variance versus time plot for case (*c*) in figure 2. The line demarcating the oscillating and the stable regimes is identified as $t = 0.46\, t_d$ (for case (*c*)).

Second, numerical investigation confirms that the oscillation in D_{eff} of a species continues until the variance of concentration distribution (which grows over time) and the square of thermal wavelength are of the same order ($\sigma^2 \sim \lambda^2$). Thereafter D_{eff} becomes steady regardless of Pe_0. For all practical purposes, hence, we recognize that D_{eff} becomes flat at an instant when the variance equals half of the square of the thermal wavelength, i.e. $\sigma^2 = \lambda^2/2$. This is demonstrated in figure 3, which corresponds to the case in figure 2*c*. The above demarcation between the oscillating and the stable regimes are obtained by synthesizing a large number of simulation results over a wide range of Pe.

Another important aspect of the dispersion phenomena studied here is the prediction of the time period of dispersivity oscillation. From figure 2, it is evident that the dimensionless time period (t^*) of oscillation of D_{eff} decreases as Pe_0 increases. Extensive numerical investigations are carried out to estimate the variation of t^* and the result is presented in figure 4. Physical parameter values for different cases presented in figure 4 are shown in table 2. All the cases in figure 4 adhere to $h \sim \delta_t$, that is, the channel height is of the same order as the thermal penetration depth. It turns out that the time period t^* varies inversely with the product of Pe_0 and the length-scale ratio, h/λ. Remarkably, the slope of the straight line joining the data points in figure 4 is exactly (–1) in the moderate Peclet number regime ($1 < \text{Pe}_0 < 100$). This result essentially means that the time period of oscillation of D_{eff} is prescribed by

$$\tau_o = t_d\, \mathrm{t}^* = \frac{\lambda}{\overline{U}},$$

where λ is the wavelength of the imposed temperature wave and $\overline{U}$ is the cross-sectional average of the net flow velocity. The characteristic time scale of the periodic variation of D_{eff} (i.e. $\tau_o = \lambda/\overline{U}$) turns out to be much larger than the time period ($t_u = \lambda/c$) of the thermal wave. An appropriate scale for the net velocity ($\overline{U}$) in the microchannel has been derived in our previous work [12] as

$$\overline{U}_s \sim \beta_T \eta_T (\Delta T)^2 c,$$

where β_T is the volumetric thermal expansion coefficient $= -(1/\rho_0)(\mathrm{d}\rho/\mathrm{d}T)$, η_T is the thermal viscosity coefficient of the fluid $= -(1/\mu_0)(\mathrm{d}\mu/\mathrm{d}T)$, and ΔT and c are the amplitude and speed of the thermal wave, respectively. Here, β_T, η_T, ρ_0 and μ_0 are evaluated at the mean temperature T_0.

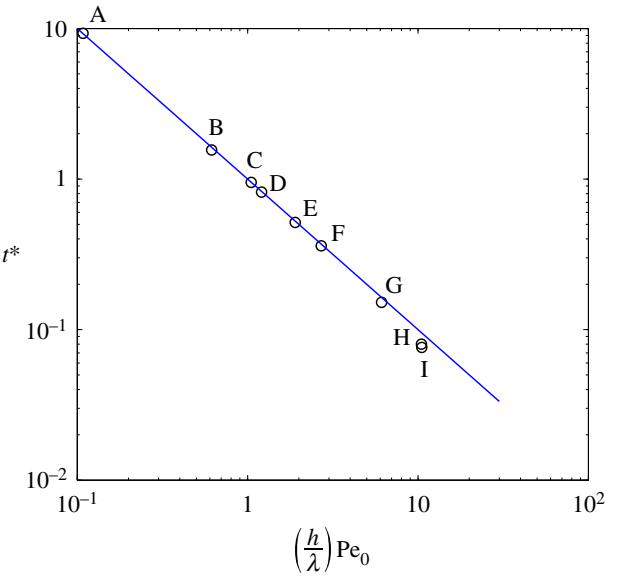

Figure 4. Time period of oscillation of axial dispersivity in the moderate Peclet number regime, i.e. $O(1) < \mathrm{Pe}_0 < O(100)$; input parameter values for cases A–I are provided in table 2. The Pe_0 values have been calculated from the numerically obtained $\overline{U}$. (Online version in colour.)

Table 2. Physical parameter values used for the computation of results in figure 4.

case	h (μm)	λ (μm)	D_0 ($m^2\,s^{-1}$)	ΔT (K)	c ($m\,s^{-1}$)	Pe_0
A	10	100	10^{-9}	20	0.1	1.1
B	10	200	10^{-11}	5	0.2	12.3
C	10	100	10^{-10}	20	0.1	10.5
D	8	150	10^{-11}	7	0.234	22.7
E	10	200	10^{-11}	8.5	0.2	38
F	10	200	10^{-11}	10	0.2	54
G	12.5	165	4×10^{-12}	10	0.1	80.8
H	10	100	10^{-11}	20	0.1	105
I	10	200	10^{-11}	20	0.2	210

At sufficiently large time (i.e. when $\sigma^2 \geq \lambda^2/2$), as the oscillation of D_{eff} dies down irrespective of the Pe_0 value, we achieve the so-called stable regime. The numerically obtained D_{eff} in the stable regime agrees well with the theoretically obtained Taylor–Aris dispersivity (refer to equation (2.8)), as shown in figure 5. Such a result is truly a confirmation of the parabolic shape of the net velocity profile for flow induced by thermoviscous actuation in a microchannel having $h \sim \delta_t$. The agreement of data presented in figure 5 serves as an essential validation of the present work as it is primarily a numerical study.

Careful inspection of figure 2 reveals that, over a very short time scale (say, $0 < t \leq 0.1\,t_d$), D_{eff} steeply increases. This is particularly evident from figure 2*c*, as the convective stretching of the species band at high Pe_0 propels a quick rise of the variance (σ^2) of the averaged concentration $\overline{C_s}$. It is obvious from the same figure that the oscillation of D_{eff} may simultaneously begin within this sharp-rise stage. Over a short time scale, suspended species particles cannot diffuse across

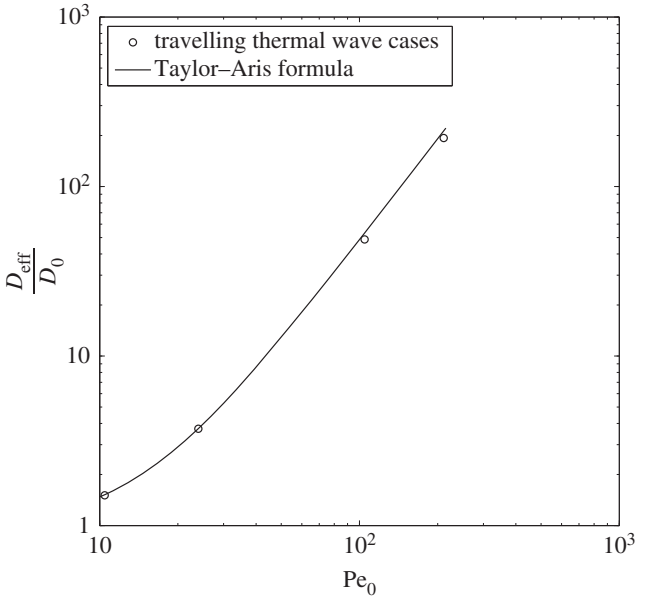

Figure 5. Comparison of long-time axial dispersion coefficients (normalized) between travelling temperature wave-induced flow in a microchannel having $h/\delta_t = 0.82$ (circular data points) and plane Poiseuille flow (solid continuous line, equation (2.8) with $\alpha = 1/210$).

the entire transverse dimension of the channel, and, thus, the dispersion is controlled by the local features of the velocity fluctuations in the channel. It was mentioned earlier that the frequency of temperature–density–pressure pulsation in flow induced by thermoviscous actuation is extremely high (time period, $\lambda/c \sim 10^{-3}\text{s}{-}10^{-5}\text{s}$), and any concentration change in that time scale, which is also the smallest time scale involved in this problem, is of little or no practical interest.

5. Conclusion

We have evaluated the axial dispersion coefficient (D_{eff}) of a species for flow induced by thermoviscous pumping in a two-dimensional microchannel, for a wide range of the mean Peclet numbers (Pe_0). As the thermoviscous actuation is governed by a spatio-temporally periodic temperature field, all the fluid properties are treated as functions of temperature. Based on the differences in spreading behaviour of the species, new temporal regimes—a small-time oscillating regime and a large-time stable regime—are defined. When the channel height is of the order of the thermal penetration depth ($h \sim \delta_t$), a strong periodic variation in the evolution of D_{eff} is observed during the oscillating regime irrespective of the Pe_0 value. At sufficiently large time, i.e. when the variance of concentration distribution grows beyond the square of the thermal wavelength (precisely, $\sigma^2 \geq \lambda^2/2$), the oscillation of axial dispersivity (D_{eff}) subsides to a constant value (the so-called stable regime). As the mean Peclet number (Pe_0) increases, it takes less dimensionless time (t/t_d) for the oscillation in dispersion to gradually settle down to the stable regime value. Our analysis corroborates that the time period of oscillation in the dispersion coefficient is expressed by the time scale $\lambda/\overline{U}$, where $\overline{U}$ is the cross-sectional average of the net velocity induced by thermoviscous expansion. The results of the present study may contribute towards an improvement in microscale systems such as microreactors and DNA amplification devices, by the judicious employment of travelling temperature waves. It may also open up a new direction in mixing control over reduced length scales, without sacrificing the net throughput.

Data accessibility. The raw data corresponding to the results presented in this paper have been uploaded as the electronic supplementary material, which all readers can access.

Authors' contributions. S.C. and D.P. formulated the problem. D.P. performed the calculations. D.P. and S.C. wrote the paper.

Competing interests. We declare we have no competing interests

Funding. S.C. acknowledges the Department of Science and Technology, Government of India, for Sir J.C. Bose National Fellowship.

References

1. Taylor G. 1953 Dispersion of soluble matter in solvent flowing slowly through a tube. *Proc. R. Soc. Lond. A* **219**, 186–203. (doi:10.1098/rspa.1953.0139)
2. Taylor G. 1954 Conditions under which dispersion of a solute in a stream of solvent can be used to measure molecular diffusion. *Proc. R. Soc. Lond. A* **225**, 473–477. (doi:10.1098/rspa.1954.0216)
3. Aris R. 1956 On the dispersion of a solute in a fluid flowing through a tube. *Proc. R. Soc. Lond. A* **235**, 67–77. (doi:10.1098/rspa.1956.0065)
4. Aris R. 1959 On the dispersion of a solute by diffusion, convection, and exchange between phases. *Proc. R. Soc. Lond. A* **252**, 538–550. (doi:10.1098/rspa.1959.0171)
5. Gill WN, Sankarasubramanian R. 1970 Exact analysis of unsteady convective diffusion. *Proc. R. Soc. Lond. A* **316**, 341–350. (doi:10.1098/rspa.1970.0083)
6. Gill WN, Sankarasubramanian R. 1971 Dispersion of a non-uniform slug in time-dependent flow. *Proc. R. Soc. Lond. A* **322**, 101–117. (doi:10.1098/rspa.1971.0057)
7. Brenner H, Edwards DA. 1993 *Macrotransport processes*. Boston, MA: Butterworth-Heinemann.
8. Ajdari A, Bontoux N, Stone HA. 2006 Hydrodynamic dispersion in shallow microchannels: the effect of cross-sectional shape. *Anal. Chem.* **78**, 387–392. (doi:10.1021/ac0508651)
9. Datta S, Ghosal S. 2009 Characterizing dispersion in microfluidic channels. *Lab. Chip* **9**, 2537–2550. (doi:10.1039/b822948c)
10. Weinert FM, Kraus JA, Franosch T, Braun D. 2008 Microscale fluid flow induced by thermoviscous expansion along a traveling wave. *Phys. Rev. Lett.* **100**, 164501. (doi:10.1103/PhysRevLett.100.164501)
11. Yariv E, Brenner H. 2004 Flow animation by unsteady temperature fields. *Phys. Fluids* **16**, L95–L98. (doi:10.1063/1.1801091)
12. Pal D, Chakraborty S. 2012 Spatially uniform microflows induced by thermoviscous expansion along a traveling temperature wave: analogies with electro-osmotic transport. *Phys. Rev. E* **86**, 016321. (doi:10.1103/PhysRevE.86.016321)
13. Aris R. 1960 On the dispersion of a solute in pulsating flow through a tube. *Proc. R. Soc. Lond. A* **259**, 370–376. (doi:10.1098/rspa.1960.0231)
14. Harris HG, Goren SL. 1967 Axial diffusion in a cylinder with pulsed flow. *Chem. Eng. Soc.* **22**, 1571–1576. (doi:10.1016/0009-2509(67)80195-7)
15. Chatwin PC. 1975 On the longitudinal dispersion of passive contaminant in oscillatory flows in tubes. *J. Fluid Mech.* **71**, 513–527. (doi:10.1017/S0022112075002716)
16. Smith R. 1982 Contaminant dispersion in oscillatory flows. *J. Fluid Mech.* **114**, 379. (doi:10.1017/S0022112082000214)
17. Watson EJ. 1983 Diffusion in oscillatory pipe flow. *J. Fluid Mech.* **133**, 233–244. (doi:10.1017/S0022112083001883)
18. Yasuda H. 1984 Longitudinal dispersion of matter due to the shear effect of steady and oscillatory currents. *J. Fluid Mech.* **118**, 383–403. (doi:10.1017/S0022112084002391)
19. Hazra SB, Gupta AS, Niyogi P. 1996 On the dispersion of a solute in oscillating flow through a channel. *Heat Mass Transfer.* **31**, 249–256. (doi:10.1007/s002310050053)
20. Bandyopadhyay S, Mazumder BS. 1999 Unsteady convective diffusion in a pusatile flow through a channel. *Acta Mech.* **134**, 1–16. (doi:10.1007/BF01170300)
21. Ng CO. 2006 Dispersion in steady and oscillatory flows through a tube with reversible and irreversible wall reactions. *Proc. R. Soc. A* **462**, 481–515. (doi:10.1098/rspa.2005.1582)
22. Jansons KM. 2006 On Taylor dispersion in oscillatory channel flows. *Proc. R. Soc. A* **462**, 3501–3509. (doi:10.1098/rspa.2006.1745)
23. Caro CG. 1966 The dispersion of indicator flowing through simplified models of the circulation and its relevance to velocity profile in blood vessels. *J. Physiol.* **185**, 501–519. (doi:10.1113/jphysiol.1966.sp007999)

24. Rana J, Murthy PVSN. 2016 Unsteady solute dispersion in non-Newtonian fluid flow in a tube with wall absorption. *Proc. R. Soc. A* **472**, 20160294. (doi:10.1098/rspa.2016.0294)
25. Rana J, Murthy PVSN. 2017 Unsteady solute dispersion in small blood vessels using a two-phase Casson model. *Proc. R. Soc. A* **473**, 20170427. (doi:10.1098/rspa.2017.0427)
26. Bowden KF. 1965 Horizontal mixing in the sea due to a shearing current. *J. Fluid Mech.* **21**, 83–95. (doi:10.1017/S0022112065000058)
27. Holley ER, Harleman DRF, Fischer HB. 1970 Dispersion in homogeneous estuary flow. *J. Hydraul. Div. ASCE* **96**, 1691–1709.
28. Dragon CA, Grotberg JB. 1991 Oscillatory flow and mass transport in a flexible tube. *J. Fluid Mech.* **231**, 135–155. (doi:10.1017/S0022112091003348)
29. Hydon PE, Pedley TJ. 1993 Axial dispersion in a channel with oscillating walls. *J. Fluid Mech.* **249**, 535–555. (doi:10.1017/S0022112093001284)
30. Hydon PE, Pedley TJ. 1996 Dispersion in oscillatory channel flow with coupled transverse wall motion. *Eur. J. Mech. B/Fluids* **15**, 143–156.
31. Grotberg JB. 1994 Pulmonary flow and transport phenomena. *Annu. Rev. Fluid Mech.* **26**, 529–571. (doi:10.1146/annurev.fl.26.010194.002525)
32. Grotberg JB, Sheth BV, Mockros LF. 1990 An analysis of pollutant gas transport and absorption in pulmonary airways. *J. Biomech. Eng. Trans. ASME* **112**, 168–176. (doi:10.1115/1.2891168)
33. Jimenez C, Sullivan PJ. 1984 Contaminant dispersion in some time-dependent laminar flows. *J. Fluid Mech.* **142**, 57–77. (doi:10.1017/S0022112084000999)
34. Mukherjee A, Mazumder BS. 1988 Dispersion of contaminant in oscillatory flows. *Acta Mech.* **74**, 107–122. (doi:10.1007/BF01194345)
35. Stroock AD, Dertinger SKW, Ajdari A, Mezic I, Stone HA, Whitesides GM. 2002 Chaotic mixer for microchannels. *Science* **295**, 647–651. (doi:10.1126/science.1066238)
36. Zholkovskij EK, Masliyah JH. 2004 Hydrodynamic dispersion due to combined pressure-driven and electroosmotic flow through microchannels with a thin double layer. *Anal. Chem.* **76**, 2708–2718. (doi:10.1021/ac0303160)
37. Shaw S, Ganguly S, Sibanda P, Chakraborty S. 2014 Dispersion characteristics of blood during nanoparticle assisted drug delivery process through a permeable microvessel. *Microvasc. Res.* **92**, 25–33. (doi:10.1016/j.mvr.2013.12.007)
38. Tripathi A, Bozkurt O, Chauhan A. 2005 Dispersion in microchannels with temporal temperature variations. *Phys. Fluids* **17**, 103607. (doi:10.1063/1.2115007)
39. Shi J, Ahmed D, Mao X, Lin SCS, Lawit A, Huang TJ. 2009 Acoustic tweezers: patterning cells and microparticles using standing surface acoustic waves (SSAW). *Lab. Chip* **9**, 2890–2895. (doi:10.1039/b910595f)
40. Thevoz P, Adams JD, Shea H, Bruus H, Soh HT. 2010 Acoustophoretic synchronization of mammalian cells in microchannels. *Anal. Chem.* **82**, 3094–3098. (doi:10.1021/ac100357u)
41. Nordin M, Laurell T. 2012 Two-hundredfold volume concentration of dilute cell and particle suspensions using chip integrated multistage acoustophoresis. *Lab. Chip* **12**, 4610–4616. (doi:10.1039/c2lc40629b)
42. Augustsson P, Magnusson C, Nordin M, Lilja H, Laurell T. 2012 Microfluidic, label-free enrichment of prostate cancer cells in blood based on acoustophoresis. *Anal. Chem.* **84**, 7954–7962. (doi:10.1021/ac301723s)
43. Rednikov AY, Sadhal SS. 2011 Acoustic/steady streaming from a motionless boundary and related phenomena: generalized treatment of the inner streaming and examples. *J. Fluid Mech.* **667**, 426–462. (doi:10.1017/S0022112010004532)
44. Muller PB, Bruus H. 2014 Theoretical aspects of microchannel acoustofluidics: thermoviscous corrections to the radiation force and streaming. *Proc. IUTAM* **10**, 410–415. (doi:10.1016/j.piutam.2014.01.035)
45. Muller PB, Bruus H. 2014 Numerical study of thermoviscous effects in ultrasound-induced acoustic streaming in microchannels. *Phys. Rev. E* **90**, 043016. (doi:10.1103/PhysRevE.90.043016)
46. Huber DE, Santiago JG. 2008 Ballistic dispersion in temperature gradient focusing. *Proc. R. Soc. A* **464**, 595–612. (doi:10.1098/rspa.2007.0161)
47. Dutta D, Ramachandran A, Leighton Jr DT. 2006 Effect of channel geometry on solute dispersion in pressure-driven microfluidic systems. *Microfluid. Nanofluid.* **2**, 275–290. (doi:10.1007/s10404-005-0070-7)

48. Datta R, Kotamarthi VR. 1990 Electrokinetic dispersion in capillary electrophoresis. *AIChE J.* **36**, 916–926. (doi:10.1002/aic.690360613)
49. Griffiths SK, Nilson RH. 1999 Hydrodynamic dispersion of a neutral nonreacting solute in electroosmotic flow. *Anal. Chem.* **71**, 5522–5529. (doi:10.1021/ac990714w)
50. Griffiths SK, Nilson RH. 2000 Band spreading in two-dimensional microchannel turns for electrokinetic species transport. *Anal. Chem.* **72**, 5473–5482. (doi:10.1021/ac000595g)
51. Ghosal S. 2006 Electrokinetic flow and dispersion in capillary electrophoresis. *Annu. Rev. Fluid Mech.* **38**, 309–338. (doi:10.1146/annurev.fluid.38.050304.092053)
52. Paul S, Ng CO. 2012 Dispersion in electroosmotic flow generated by oscillatory electric field interacting with oscillatory wall potentials. *Microfluid. Nanofluid.* **12**, 237–256. (doi:10.1007/s10404-011-0868-4)
53. Pal D, Chakraborty S. 2015 Fluid flow induced by periodic temperature oscillation over a flat plate: comparisons with the classical Stokes problems. *Phys. Fluids* **27**, 053601. (doi:10.1063/1.4919733)
54. Edward JT. 1970 Molecular volumes and the Stokes-Einstein equation. *J. Chem. Educ.* **47**, 261–270. (doi:10.1021/ed047p261)
55. James SC, Chrysikopoulos CV. 2003 Effective velocity and effective dispersion coefficient for finite-sized particles flowing in a uniform fracture. *J. Colloid Interface Sci.* **263**, 288–295. (doi:10.1016/S0021-9797(03)00254-6)
56. Patankar SV. 1980 *Numerical heat transfer and fluid flow*. New York, NY: McGraw-Hill.
57. Versteeg HK, Malalasekera W. 2007 *An introduction to computational fluid dynamics: the finite volume method*. London, UK: Prentice Hall.
58. White FM. 2011 *Fluid mechanics*. New York, NY: McGraw-hill.
59. Xuan X, Xu B, Sinton D, Li D. 2004 Electroosmotic flow with Joule heating effects. *Lab. Chip* **4**, 230–236. (doi:10.1039/b315036d)
60. Squires T, Quake S. 2005 Microfluidics: fluid physics at the nanoliter scale. *Rev. Mod. Phys.* **77**, 977–1026. (doi:10.1103/RevModPhys.77.977)